

Supplemental Material

Ultrafast Electron Injection to Photo-Excited Organic Molecules

Dean Cvetko,^{1,2,3,*} Guido Fratesi,^{4,5,†} Gregor Kladnik,^{1,3} Albano Cossaro,³

Gian Paolo Brivio,⁵ Latha Venkataraman,^{6,7,‡} and Alberto Morgante^{3,8}

¹*Physics Department, Faculty of Mathematics and Physics, University of Ljubljana, Slovenia*

²*Jozef Stefan Institute, Ljubljana, Slovenia*

³*CNR-IOM, Laboratorio TASC, Basovizza, Trieste, Italy*

⁴*Dipartimento di Fisica, Università degli Studi di Milano, Italy*

⁵*Dipartimento di Scienza dei Materiali, Università di Milano-Bicocca, Italy*

⁶*Department of Applied Physics, Columbia University, New York, NY.*

⁷*Department of Chemistry, Columbia University, New York, NY.*

⁸*Dipartimento di Fisica, Università di Trieste, Italy*

(Dated: June 3, 2016)

CONTENTS

| | |
|--|----|
| Experimental Details and Sample Preparation | 2 |
| X-ray Photoemission Spectroscopy and Near Edge X-ray Absorption Fine Structure | 2 |
| Charge Transfer Dynamics Calculation Details | 6 |
| Additional Theoretical Details | 11 |
| References | 14 |

EXPERIMENTAL DETAILS AND SAMPLE PREPARATION

The experiments have been performed at the ALOISA and ANCHOR endstations of the ALOISA beamline [1] at the Elettra synchrotron in Trieste, Italy. The Au(111) substrate was prepared by repeated cycles of Ar+ sputtering and annealing at 750K. X-ray photoemission spectroscopy (XPS) was used to check for any chemical impurities (O, N, and C). Pyridine (PYR, Sigma-Aldrich) was placed in a pyrex container and attached through a leak valve to the UHV experimental chamber maintained at pressures of $10^{-10} - 10^{-11}$ mbar. The PYR/Au(111) multilayer was produced by PYR gas condensation in $10^{-7} - 10^{-6}$ mbar atmosphere on the Au(111) substrate, kept at 200K. Flash-heating this multilayer film to temperatures ranging from -60°C to 0°C yielded PYR monolayer films with variable adsorption geometries as detailed in the main text.

X-RAY PHOTOEMISSION SPECTROSCOPY AND NEAR EDGE X-RAY ABSORPTION FINE STRUCTURE

XPS measurements were performed with the X-ray beam at grazing-incidence (4°) to the sample. Photoelectrons from the sample were collected at the normal to the surface using a hemispherical electron analyzer with an acceptance angle of 2° , and an overall energy resolution of ~ 0.2 eV. The energy scale for XPS spectra was calibrated by aligning the Au $4f_{7/2}$ peak to a binding energy of 84.0 eV. XPS experiments were performed with photon energy of 500 eV to obtain core-excitation spectra and 130 eV for valence band (VB) spectra.

Fig. S1 shows C1s and N1s XPS for the PYR multilayer and the monolayer film with the molecules making an angle of $\sim 59^{\circ}$ to the surface. The multilayer XPS spectra show a single N1s peak at a binding energy $E_{N1s} = 400$ eV. The C1s peak at $E_{C1s} = 286$ eV is broadened as the carbons bonded to the N atom are chemically nonequivalent to the other carbons. Core level binding energy shifts of approximately ~ -0.8 eV are observed for monolayer films due to final state screening of the core hole by the Au substrate [2].

Near edge X-ray absorption fine structure (NEXAFS) measurements were performed on the nitrogen (carbon) K-edge by sweeping the incident photon energy from 396 eV to 420 eV (280 eV to 315 eV) in steps of 0.1 eV. The photon incidence angle was set to 6° . Spectra were acquired using a channeltron detector with a wide acceptance angle in the partial electron

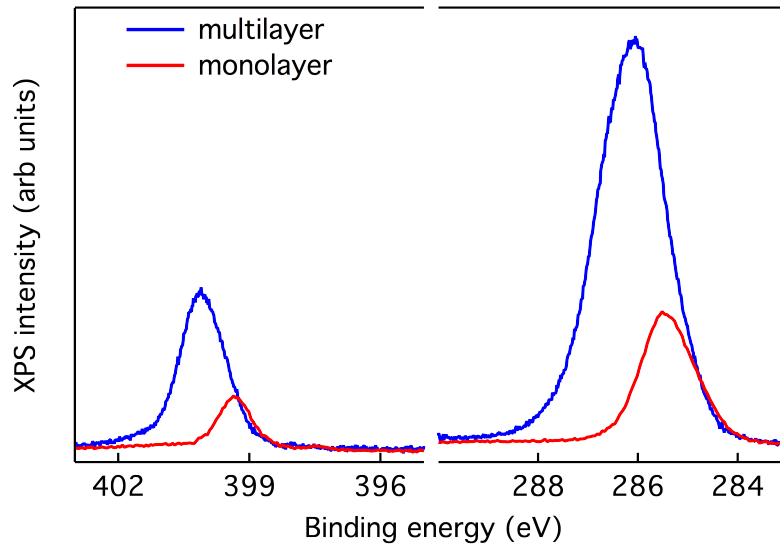


FIG. S1. Carbon and Nitrogen XPS of PYR multilayer (blue curve) and monolayer (red curve, 59° tilt angle) taken with photon energy of 500 eV. A 0.8 eV Au-induced screening shift of the core hole is clearly visible.

yield mode and a high pass filter with cutoff energy set to 370 eV (or 250 eV). The photon flux was monitored on the last optical element along the beam path. The sample normal was oriented either parallel (p-pol) or perpendicular (s-pol) to the light polarization, or kept at the magic angle (with the \vec{E} -field tilted by 54.7° from the surface normal).

The C and N K-edge NEXAFS for the monolayer PYR film (59°) are shown Fig. S2A by aligning the photon energy scales at the C1s and N1s XPS peaks. We note that LUMO peaks in the two NEXAFS spectra coincide with this alignment. This reflects the fact that due to proximity of the metallic substrate the core hole on the molecule, induced by XPS, is efficiently screened by the gold substrate [3], indicating a relatively good molecule-metal coupling.

Resonant valence band (VB) spectra of the PYR monolayer, taken at the C1s \rightarrow LUMO* and N1s \rightarrow LUMO* resonances are also shown in Fig. S2B. Several resonances (e.g. at 5 eV, 7.5 eV, 11 eV) are visible, and correspond to core electron excitation to the LUMO and subsequent de-excitation with electron emission, leaving a hole in an occupied molecular orbital. The multilayer VB resonant spectra are also shown. Isodensity plots of the HOMO and LUMO wave function obtained from DFT calculations for the isolated molecule are

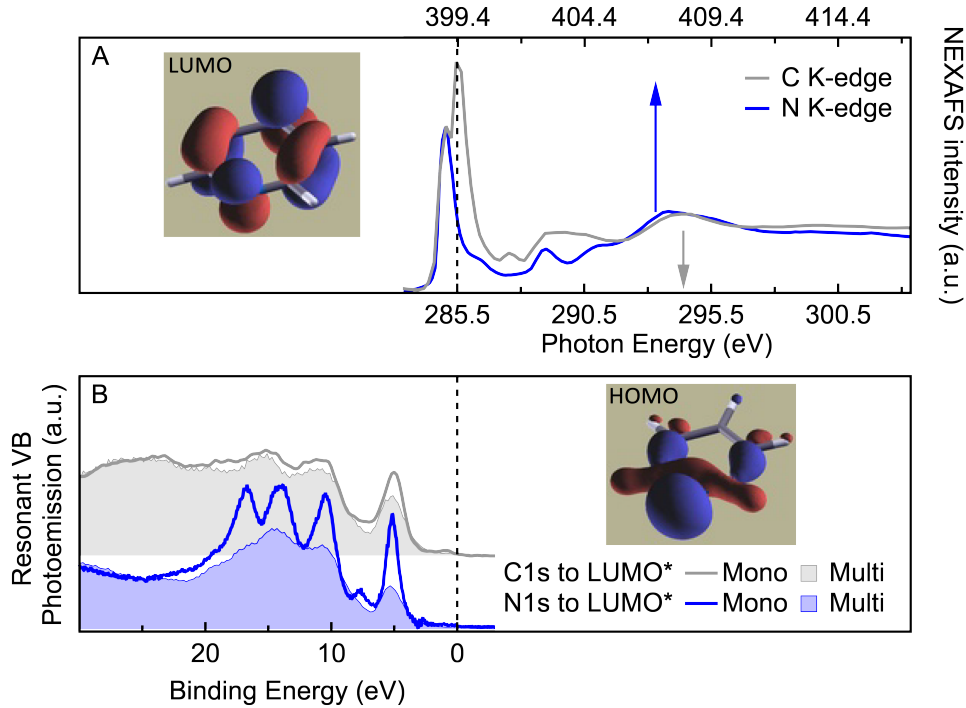


FIG. S2. (A) Monolayer C and N K-edge NEXAFS shown aligning the photon energy scales at the XPS peak locations (C1s XPS peak at 285.5 eV and N1s XPS peak at 399.4 eV). Calculated LUMO orbital, with weight on both C and N atoms is also shown. (B) Resonant VB photoemission spectra at C1s \rightarrow LUMO* and N1s \rightarrow LUMO* resonance for both monolayer and multilayer films. Note that the multilayer spectra have been offset by ~ 2 eV to lower binding energies to account for the screening shift of the monolayer film. Calculated HOMO orbital is also shown.

shown in the inset of the Fig. S2. Calculated LUMO and HOMO orbitals are distributed over C and N sites in agreement with the fact that strong VB resonances are observed for this orbital pair on either core excitation site.

Detailed orbital assignment of the NEXAFS spectra can be performed following the DFT calculated electronic structure (Fig. S3). For these calculations, we use GPAW, a grid-based real-space projector-augmented-wave (PAW) code, with the BLYP exchange-correlation functional [4, 5]. For these simulations, isolated molecules were first relaxed to their optimized geometries. Default grid spacings and convergence thresholds were employed. All NEXAFS calculations were performed using the half-core-hole approximation [6]. The absolute energy scale was determined by performing a delta Kohn-Sham calculation and

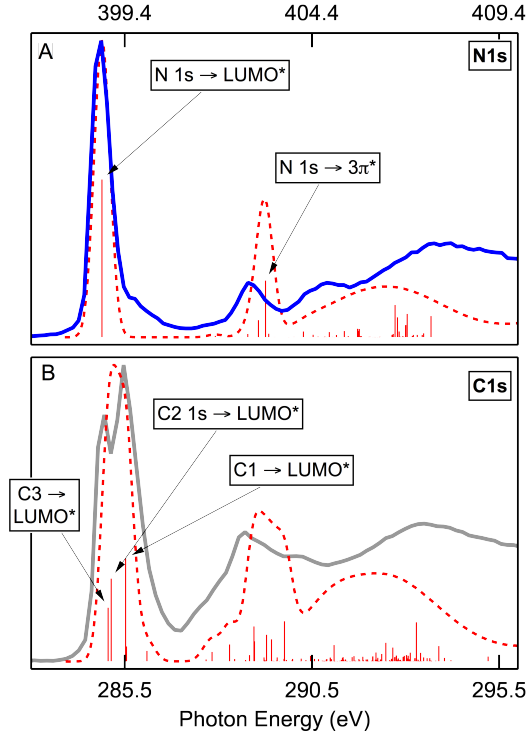


FIG. S3. DFT calculated NEXAFS of isolated PYR at (A) N K-edge and (B) C K-edge. Principal transitions are shown as vertical bars. The overall spectrum with Gaussian broadening (FWHM=0.3 eV) is shown as a dashed line and compared to experimental data (full line).

shifting the computed spectrum using the calculated total energy difference between the ground and the first core excited state.

Molecular Tilt Calculations

The relative intensity of the NEXAFS signal in s-pol and p-pol for the C1s to LUMO transition was used to obtain the orientation of the aromatic ring relative to the surface for each monolayer film. The angle θ of the ring to the surface is determined using the relation:

$$\tan \theta = \sqrt{\frac{2I_{\pi}^s}{I_{\pi}^p}}$$

where I_{π}^s and I_{π}^p are the intensities of the LUMO (π^*) NEXAFS peak from the s-pol and p-pol spectra respectively. Alternatively, since we also measure the NEXAFS intensity of the LUMO π^* and σ^* peaks with the surface inclined at the magic angle $\theta = 54.7^{\circ}$ (I_{π}^{mag}

and I_σ^{mag}), we can obtain the average angle from:

$$\tan \theta = \sqrt{2 \frac{I_\pi^{mag} I_\sigma^p}{I_\sigma^{mag} I_\pi^p}}.$$

In practice, we normalize the NEXAFS spectrum measured in p-pol to the intensity of the σ^* peak measured at the magic angle and deduce the molecular angle from $\tan \theta = \sqrt{2I_\pi^{mag}/I_\pi^p}$. This procedure has the advantage that we only need to measure a single NEXAFS spectrum in the multilayer with random molecular orientation or at magic angle configuration and then determine the molecular tilt angle from the p-pol spectra alone.

CHARGE TRANSFER DYNAMICS CALCULATION DETAILS

We first consider the energy level alignment of the molecular orbitals (MO) relative to the Fermi level (E_F) of the Au metallic substrate. In the ground state (GS) the LUMO and higher unoccupied MOs are above E_F . Upon X-ray absorption the MOs in the presence of the core-exciton (core hole plus an electron in an unoccupied MO) are shifted down by an energy ΔE . As a consequence, the LUMO*, that is broadened due to hybridization with the Au surface, may be partially below E_F of the substrate. In such a situation, conventional CHC analysis method must be modified to describe the bi-directional charge transfer between the molecule and metal surface.

Core \rightarrow LUMO excitation calculation

We follow the method described in detail in Bruhwiler et al. [7], with a key difference, which is to consider that a fraction of the LUMO* is below E_F . We denote this fraction as x . We first consider core \rightarrow LUMO excitation (Fig. S4a). Such system decays without charge transfer (CT) from the LUMO* to the substrate with a probability P_{NoCT} given as:

$$P_{NoCT} = \underbrace{x}_{\text{fraction} < E_F} + \int_0^\infty \frac{\Gamma_{ch}}{\hbar} e^{-\Gamma_{ch}t/\hbar} (1-x) \underbrace{\left[1 - \int_0^t \frac{\Gamma_{CT}}{\hbar} e^{-\Gamma_{CT}t'/\hbar} dt' \right]}_{\text{fraction} > E_F} dt \quad (1)$$

$$= x + (1-x) \int_0^\infty \frac{\Gamma_{ch}}{\hbar} e^{-(\Gamma_{CT}+\Gamma_{ch})t/\hbar} dt = \quad (2)$$

$$\boxed{P_{NoCT} = x + (1-x) \frac{\Gamma_{ch}}{\Gamma_{ch} + \Gamma_{CT}}} \quad (3)$$

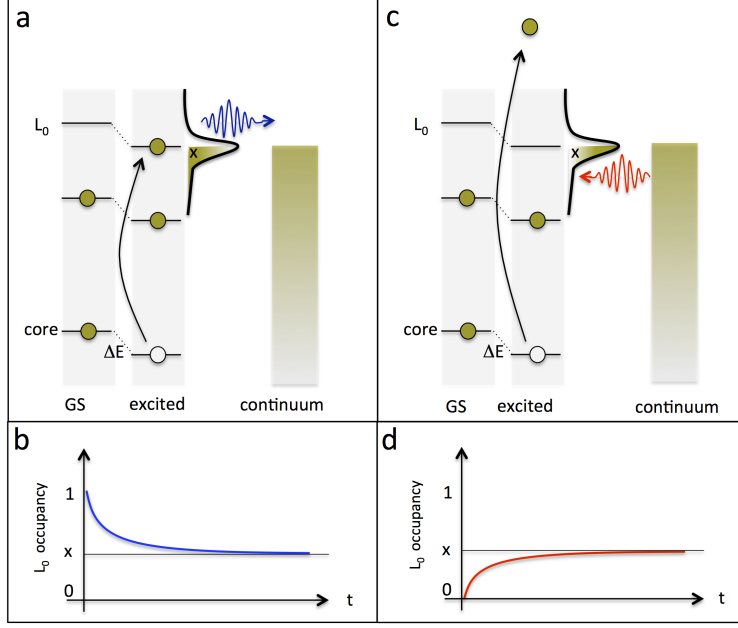


FIG. S4. Schematics of electron transfer dynamics from/to the LUMO* upon core electron excitation to a) LUMO and c) free-electron continuum. The respective LUMO* populations as a function of time after core-hole creation are schematically illustrated in b) and d).

where Γ_{CT} , and Γ_{ch} are related to the inverse of the characteristic time constants as $\tau_{CT} = \hbar/\Gamma_{CT}$ and $\tau_{ch} = \hbar/\Gamma_{ch}$ for charge transfer and core-hole decay, respectively. Since x is the fraction of the LUMO* that is below E_F , it also implies that the probability of having no charge transfer is increased by x , hence the first term in Eq. 1. Additionally, the fraction above E_F (i.e. $1 - x$) is included as a prefactor, since it is only this fractional occupation that can compete with the core-hole decay channel.

Similarly, the expression for the core-hole decay probability with charge transfer P_{CT} (i.e. with the LUMO* electron delocalizing to the substrate occurring prior to the core-hole decay) is:

$$P_{CT} = \int_0^\infty \underbrace{\frac{\Gamma_{ch}}{\hbar} e^{-\Gamma_{ch}t/\hbar}}_{\text{core-hole decay}} \left[(1-x) \underbrace{\int_0^t \frac{\Gamma_{CT}}{\hbar} e^{-\Gamma_{CT}t'/\hbar} dt'}_{\text{CT prior to core-hole decay}} \right] dt \quad (4)$$

$$\boxed{P_{CT} = (1-x) \frac{\Gamma_{CT}}{\Gamma_{ch} + \Gamma_{CT}}} \quad (5)$$

Of course, $P_{CT} + P_{NoCT} = 1$ and for LUMO* fully above E_F ($x = 0$), the conventional CHC

expressions are recovered:

$$P_{CT} = \frac{\Gamma_{CT}}{\Gamma_{ch} + \Gamma_{CT}} \quad \text{and} \quad P_{NoCT} = \frac{\Gamma_{ch}}{\Gamma_{CT} + \Gamma_{ch}}$$

For $x = 1$, the LUMO* is fully below E_F and we get $P_{NoCT} = 1$. Therefore the participator intensity in this case is equal to that of an isolated system. Following Bruhwiler et al. [7], we can relate the probabilities P_{CT} and P_{NoCT} to the RPES intensities as:

$$\frac{P_{NoCT}}{P_{CT}} = \frac{I_p + I_{Raman}}{I_{Auger}} \propto \frac{I_p}{I_{Auger}} = \frac{\Gamma_{ch} + x \cdot \Gamma_{CT}}{(1-x)\Gamma_{CT}} \quad (6)$$

where I_p , I_{Auger} and I_{Raman} denote the intensities of the participator, Raman Auger (i.e. spectator shifted Auger) and normal Auger peak in the RPES spectrum of the molecule on Au (coupled system). Analogous intensities for the isolated system (either gas phase or multilayer films) can also be defined as I_p^0 , I_{Auger}^0 and I_{Raman}^0 . For this coupled system where the electronic structure of the molecule is only weakly perturbed relative to that of the isolated molecule, we consider $I_p + I_{Raman} \propto I_p$, and use I_p in place of $I_p + I_{Raman}$. Again for $x = 0$ we obtain the conventional expression $P_{NoCT}/P_{CT} = \Gamma_{ch}/\Gamma_{CT}$ [7, 8]. The above relation may be simplified to

$$I_{Auger}\Gamma_{ch} = [(1-x)I_p - x \cdot I_{Auger}] \Gamma_{CT} \quad (7)$$

yielding for the CT time:

$$\tau_{CT} = \tau_{ch} \left[\frac{I_p}{I_{Auger}} \cdot (1-x) - x \right]. \quad (8)$$

We remember that in both coupled and isolated system, the overall intensities scale as $I_p + I_{Auger} = I_p^0 + I_{Auger}^0 = I_p^0$, so we obtain

$$\tau_{CT} = \tau_{ch} \left(\frac{I_p}{I_p^0 - I_p} - \frac{x I_p^0}{I_p^0 - I_p} \right) \quad (9)$$

The first term in Eq. (9) is the conventional expression of the CHC CT time. The second term is the correction which takes into account the probability for an electron on the LUMO* to delocalize to the substrate is x . Note that this implies that the fraction I_p/I_p^0 is greater than x .

Core \rightarrow free-electron-continuum excitation calculation

Next we consider the excitation of the core electron into the free electron continuum above the ionization threshold. The LUMO* in the presence of the core-hole is also shifted down in energy by ΔE relative to ground state (Fig. S4C) thus it is again partially below E_F . We again denote the fraction of the LUMO* that is below E_F as x . Since the LUMO* is initially empty, it may get populated by charge transfer from the Au substrate on the timescale of the core-hole decay. This will allow for the super-participator channel in addition to the normal Auger as discussed in the main text. The relative intensities of these two decay channels reflects the dynamics of the electron transfer from the substrate to the LUMO*. We therefore extend the CHC analysis to include the competition between the core-hole decay channels with and without the electron transfer from Au to the LUMO*. We then obtain a core-hole decay probability following electron back-transfer from the substrate as:

$$P_{BT} = \int_0^\infty \underbrace{\frac{\Gamma_{ch}}{\hbar} e^{-\Gamma_{ch}t/\hbar}}_{\text{core-hole decay}} \left[x \int_0^t \underbrace{\frac{\Gamma_{BT}}{\hbar} e^{-\Gamma_{BT}t'/\hbar} dt'}_{\text{BT prior to core-hole decay}} \right] dt \quad (10)$$

$$\boxed{P_{BT} = x \cdot \frac{\Gamma_{BT}}{\Gamma_{ch} + \Gamma_{BT}}} \quad (11)$$

and for the probability for core-hole decay without a back-transfer from the substrate as:

$$P_{NoBT} = (1 - x) + x \int_0^\infty \underbrace{\frac{\Gamma_{ch}}{\hbar} e^{-\Gamma_{ch}t/\hbar}}_{\text{core-hole decay}} \left[\underbrace{1 - \int_0^t \frac{\Gamma_{BT}}{\hbar} e^{-\Gamma_{BT}t'/\hbar} dt'}_{\text{No back-transfer}} \right] dt = \quad (12)$$

$$\boxed{P_{NoBT} = (1 - x) + x \cdot \frac{\Gamma_{ch}}{\Gamma_{ch} + \Gamma_{BT}}} \quad (13)$$

When $x = 1$ we get:

$$P_{NoBT} = \frac{\Gamma_{ch}}{\Gamma_{ch} + \Gamma_{BT}}, \quad P_{BT} = \frac{\Gamma_{BT}}{\Gamma_{ch} + \Gamma_{BT}} \quad \text{and} \quad \frac{P_{NoBT}}{P_{BT}} = \frac{\tau_{BT}}{\tau_{ch}}.$$

To relate these probabilities to measurements in the case when $x = 1$, we consider the participator and super-participator intensities measured at core \rightarrow LUMO* or core \rightarrow vacuum excitations are denoted as I_p and I_{sp} respectively. The ratio P_{NoBT}/P_{BT} is then simply $(I_p - I_{sp})/I_{sp}$. For $x = 0$ we trivially get $P_{NoBT} = 1$ and $P_{BT} = 0$.

For $0 < x < 1$, the above relations include two independent unknowns x and τ_{BT} . We need to use the intensities of the core \rightarrow LUMO* participator resonance, I_p^0 , the normal Auger, I_{Auger}^0 and spectator shifted Raman Auger, I_{Raman}^0 in an isolated system (gas phase

or multilayer). Of course in the isolated system, $I_{Auger}^0 = 0$ thus $I_p^0 \propto (I_p^0 + I_{Raman}^0)$. We obtain:

$$\frac{P_{NoBT}}{P_{BT}} = \frac{\Gamma_{ch} + (1-x)\Gamma_{BT}}{x\Gamma_{BT}} = \frac{\tilde{\tau}_{BT}}{x} + \frac{1-x}{x} \quad (14)$$

with dimensionless time $\tilde{\tau}_{BT} = \tau_{BT}/\tau_{ch}$. Since one also has

$$\frac{P_{NoBT}}{P_{BT}} = \frac{I_p^0 - I_{sp}}{I_{sp}} \quad (15)$$

the equations above result in

$$\tilde{\tau}_{BT} = \frac{x - I_{sp}/I_p^0}{I_{sp}/I_p^0}. \quad (16)$$

Determination of characteristic charge transfer time

Defining the fractions $f = I_p/I_p^0$ and $\beta = I_{sp}/I_p$ (hence $I_{sp}/I_p^0 = \beta f$), we obtain for the direct charge transfer time

$$\tilde{\tau}_{CT} = \frac{f-x}{1-f}, \quad (17)$$

and for the back-transfer time

$$\tilde{\tau}_{BT} = \frac{x - \beta f}{\beta f}. \quad (18)$$

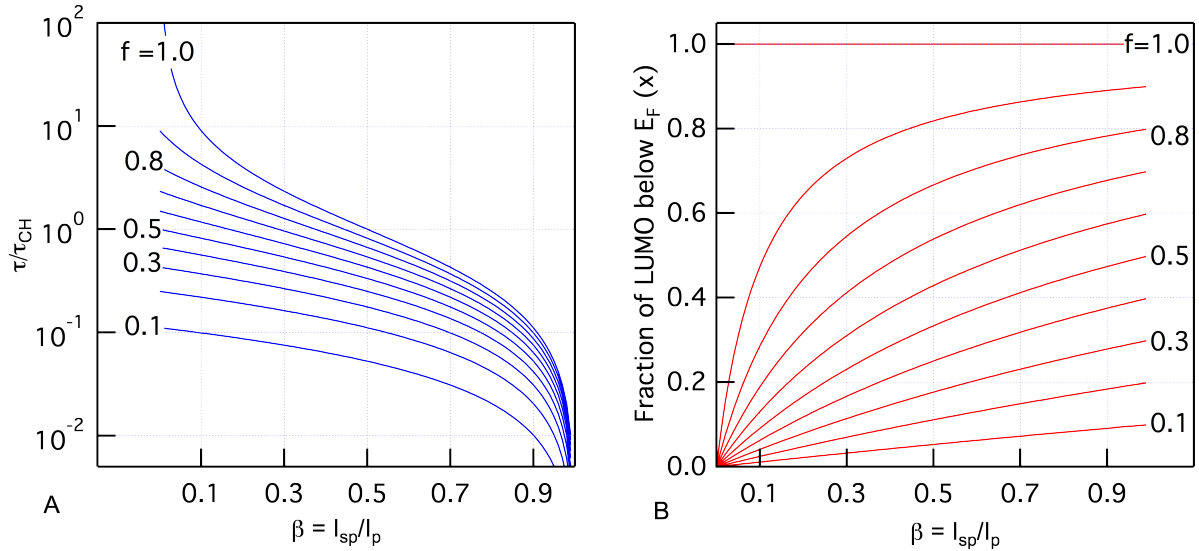


FIG. S5. Graphical representation of the dependence of $\tilde{\tau}$ (A) and x (B) on the intensity ratios $\beta = I_{sp}/I_p$ and $f = I_p/I_p^0$.

We assume that charge transfer probability is direction independent, i.e. that the characteristic times for electron delocalization from LUMO* to Au and for back-transfer from Au to the LUMO* are the same, $\tilde{\tau}_{CT} = \tilde{\tau}_{BT} = \tilde{\tau}$. Equating (17) and (18) for both charge transfer time and fractional occupancy of LUMO*, we get:

$$\tilde{\tau} = \frac{f(1 - \beta)}{1 - f(1 - \beta)} \quad (19)$$

$$x = \frac{\beta f}{1 - f(1 - \beta)} \quad (20)$$

For a graphical representation of the Eqs. (19,20) see Fig. (S5). By applying these equations we can evaluate the charge injection times from Au to the PYR molecule as a function of molecular tilt angle as reported in Fig. 3 of the main paper. At the same time we also evaluate the fraction x of the LUMO* that is partially below E_F . These latter values are found to be close to unity (0.9 ± 0.05) for all tilt angles considered, which agrees well with our theoretical predictions.

Auger peak position and fast injection of electrons

The LUMO* electron presence on the molecule during the time window of the core-hole decay can be further evidenced in the kinetic energy of the Auger peaks. Fig. S6 shows the N RPES for multilayer (upper panel) and monolayer (lower panel) with single scans at the core \rightarrow LUMO (red color curves) and core \rightarrow free electron continuum (black curves) excitations, shown in the central panel. For the multilayer we see the Auger peak at the core \rightarrow LUMO excitation shifted to higher kinetic energies because of the Coulomb screening by the LUMO* electron. For the monolayer, the Auger peaks for both, core \rightarrow LUMO and core \rightarrow free electron continuum spectra, are found at the same, blue shifted kinetic energy, evidencing that LUMO* is always occupied. For the latter excitation this indicates, that ultrafast injection from Au to the pyr molecule occurs prior to the core-hole decay.

ADDITIONAL THEORETICAL DETAILS

The resonant charge transfer time τ from a molecular state Φ is determined as $\tau = \hbar/\Gamma$ [9, 10] from the Lorentzian full width at half-maximum (fwhm) Γ in the density of states projected onto that orbital:

$$\rho_{\Phi}(E) = \frac{1}{\pi} \text{Im} [G_{\Phi\Phi}(E)] \propto \frac{1}{\pi} \frac{(\Gamma + \gamma)/2}{(E - E_{\Phi})^2 + [(\Gamma + \gamma)/2]^2} \quad (21)$$

with E_Φ and Γ as fitting parameters, $G_{\Phi\Phi}(E)$ the expectation value of the Green's function on the Φ state, and $\gamma = 4$ meV an additional broadening added for computational convenience.

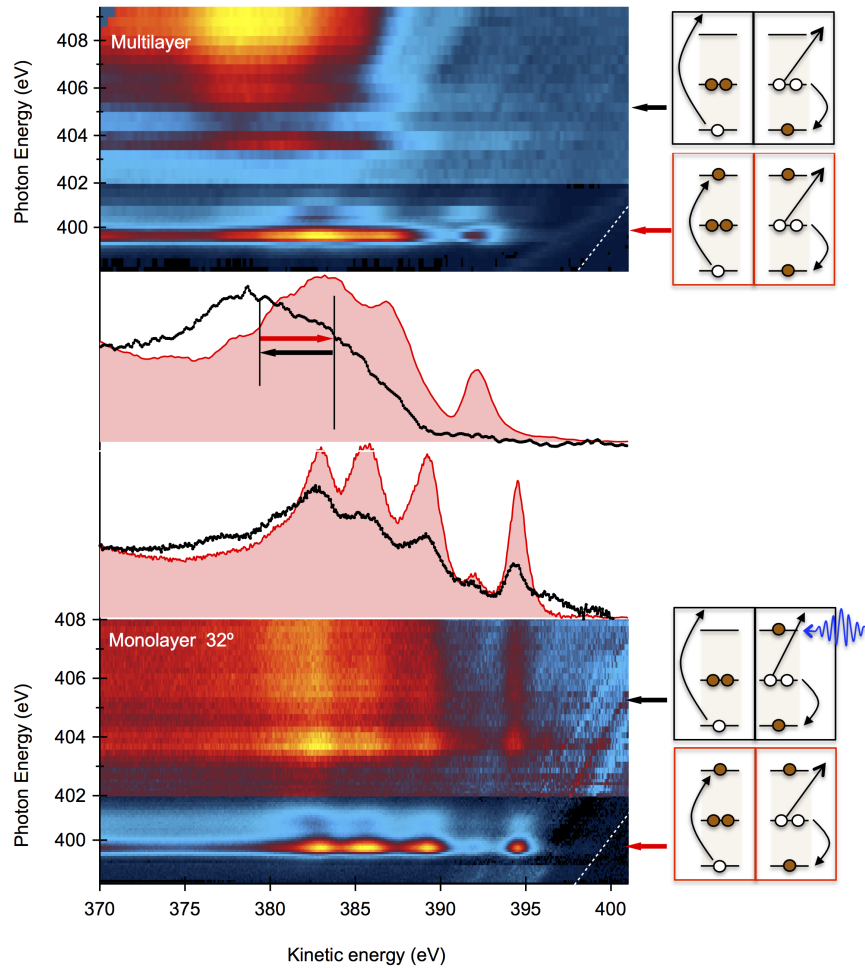


FIG. S6. Nitrogen K-edge RPES for pyridine multilayer (upper panel) and pyridine monolayer on Au (lower panel). Different color scales are used for the 398-402 eV and 402-410 eV photon energy ranges to emphasize the contrast of the super participator lines above 402 eV. Single scans at core \rightarrow LUMO ($h\nu=399.5\text{eV}$, filled red curve) and at core \rightarrow free electron continuum ($h\nu=405\text{ eV}$, black curve), indicated by respective red and black arrows are shown in the middle panel. Spectator shift of the Auger peak due to LUMO* electron is seen between the multilayer spectra at 399.5 eV and 405 eV. For monolayer, the 399.5 and 405 eV spectra, show no such shift between the Auger peaks, indicating the similar occupation of LUMO* in both cases. Schematic energy level diagram with the Auger emission and the LUMO* occupation is depicted aside.

* Dean.Cvetko@fmf.uni-lj.si

† guido.fratesi@unimi.it

‡ lv2117@columbia.edu

- [1] L. Floreano, G. Naletto, D. Cvetko, R. Gotter, M. Malvezzi, L. Marassi, A. Morgante, A. Santaniello, A. Verdini, F. Tommasini, and G. Tondello, *Review of Scientific Instruments*, **70**, 3855 (1999), ISSN 00346748.
- [2] N. V. Smith, C. T. Chen, and M. Weinert, *Physical Review B*, **40**, 7565 (1989), ISSN 01631829.
- [3] N. Mårtensson, a. B. Preobrajenski, and F. Hennies, *The European Physical Journal Special Topics*, **169**, 133 (2009), ISSN 1951-6355.
- [4] J. Enkovaara, C. Rostgaard, J. J. Mortensen, J. Chen, M. Duak, L. Ferrighi, J. Gavnholt, C. Glinsvad, V. Haikola, H. a. Hansen, H. H. Kristoffersen, M. Kuisma, a. H. Larsen, L. Lehtovaara, M. Ljungberg, O. Lopez-Acevedo, P. G. Moses, J. Ojanen, T. Olsen, V. Petzold, N. a. Romero, J. Stausholm-Møller, M. Strange, G. a. Tritsarlis, M. Vanin, M. Walter, B. Hammer, H. Häkkinen, G. K. H. Madsen, R. M. Nieminen, J. K. Nørskov, M. Puska, T. T. Rantala, J. Schiøtz, K. S. Thygesen, and K. W. Jacobsen, *Journal of physics. Condensed matter : an Institute of Physics journal*, **22**, 253202 (2010), ISSN 0953-8984.
- [5] M. Ljungberg, J. Mortensen, and L. Pettersson, *Journal of Electron Spectroscopy and Related Phenomena*, **184**, 427 (2011), ISSN 03682048.
- [6] M. Cavalleri, M. Odelius, D. Nordlund, A. Nilsson, and L. G. M. Pettersson, *Physical chemistry chemical physics : PCCP*, **7**, 2854 (2005), ISSN 1463-9076.
- [7] P. A. Brühwiler, O. Karis, and N. Mårtensson, *Reviews of Modern Physics*, **74**, 703 (2002), ISSN 0034-6861.
- [8] D. Menzel, *Chemical Society reviews*, **37**, 2212 (2008), ISSN 0306-0012.
- [9] S. Datta, *Quantum Transport - Atom to Transistor* (Cambridge University Press, 2005).
- [10] A. Nitzan, *Chemical Dynamics in Condensed Phases: Relaxation, Transfer and Reactions in Condensed Molecular Systems* (Oxford University Press, 2006) ISBN 0-19-852979-1.